Mode- and Size-Dependent Landau-Lifshitz Damping in Magnetic Nanostructures: Evidence for Nonlocal Damping

Hans T. Nembach, Justin M. Shaw, Carl T. Boone, and T. J. Silva

Electromagnetics Division, National Institute of Standards and Technology, Boulder, Colorado 80305, USA

(Received 10 September 2012; revised manuscript received 23 November 2012; published 12 March 2013)

We demonstrate a strong dependence of the effective damping on the nanomagnet size and the particular spin-wave mode that can be explained by the theory of intralayer transverse-spin pumping. The effective Landau-Lifshitz damping is measured optically in individual, isolated nanomagnets as small as 100 nm. The measurements are accomplished by use of a novel heterodyne magneto-optical microwave microscope with unprecedented sensitivity. Experimental data reveal multiple standing spin-wave modes that we identify by use of micromagnetic modeling as having either localized or delocalized character, described generically as end and center modes. The damping parameter of the two modes depends on both the size of the nanomagnet as well as the particular spin-wave mode that is excited, with values that are enhanced by as much as 40% relative to that measured for an extended film. Contrary to expectations based on the *ad hoc* consideration of lithography-induced edge damage, the damping for the end mode decreases as the size of the nanomagnet decreases. The data agree with the theory for damping caused by the flow of intralayer transverse spin currents driven by the magnetization curvature. These results have serious implications for the performance of nanoscale spintronic devices such as spin-torque-transfer magnetic random access memory.

DOI: 10.1103/PhysRevLett.110.117201 PACS numbers: 75.75.−c, 75.40.Gb, 75.50.Tt, 75.60.Ej

The Landau-Lifshitz and Gilbert equations [1–3], both with purely local formulations of the damping term, are regarded as the definitive phenomenological descriptions of dissipative ferromagnetic dynamics. Most micromagnetic simulations for magnetization dynamics rely on the local damping formulation in a diverse variety of systems, e.g. disk drives [4], telecommunications [5], and biomolecule sorting [6]. However, an outstanding question is damped gyromagnetic precession subject to finite size effects at the nanometer scale: Should one expect damping to be identical for a 10 nm and a 10 cm body, all else being equal? The answer to this question is of great technological significance for a broad range of applications. For example, the damping parameter α is a critical figure of merit for the efficient operation of many spintronic devices, e.g., spin-torque-transfer magnetic random access memory (STT-MRAM) devices that are potentially scalable down to the 22 nm lithography node and beyond [7]. In the case of STT-MRAM, the switching energy scales quadratically with switching current, which is in turn proportional to α; thus, small α is essential for low power operation.

The leading theory for damping in ferromagnetic conductors is magnon-electron scattering [8,9], whereby intrinsic damping is purely local at room temperature [10]. To date, spin-pumping, which drives spin current from a ferromagnet into adjacent nonmagnetic conducting layers, is the only experimentally confirmed mechanism of extrinsic nonlocal damping [11]. Recent theoretical work describes *intrinsic* nonlocal damping due to the dissipative flow of nonequilibrium *intralayer* spin currents within the ferromagnet itself [12–15], which can give rise to enhanced damping in isolated magnetic nanostructures. Evidence in support of such theories remains inconclusive. Experimentally, spin-torque ferromagnetic resonance (ST-FMR) has been widely used to measure damping in individual nanoscale devices. While the damping is often found to be larger than values reported for extended thin films (measured damping values for Permalloy in nanopillars by use of ST-FMR range from 0.010 ± 0.002 at room temperature [16] to 0.016 at 4.2 K [17]; the intrinsic α for thin film Permalloy is only 0.004 ± 0.001 [18]), this discrepancy has often been attributed to increased damping close to the edges of the nanomagnets, the result of damage, redeposition and/or oxidation at the sidewalls [17]. Unfortunately, the interpretation of ST-FMR data is made difficult by the complexity of the multilayer structures, Oersted field effects, and the difficulty in isolating the contributions to damping from interlayer interactions. We now demonstrate that intrinsic nonlocal effects, moderated by spin-wave mode confinement, are important contributors to damping in magnetic nanostructures. Indeed, we show that both interlayer and intralayer spin pumping are of comparable magnitude for the nanoscale systems considered here.

Our approach is to measure the dynamics in individual nanomagnets with a single ferromagnetic layer. This allows determination of the intrinsic properties of the quantized spin-wave modes without influence of other adjacent ferromagnetic layers. Extraction of α from ensemble measurements of nanomagnet arrays is not trivial, both because (a) the resonance frequencies might differ from nanomagnet to nanomagnet [19,20], and (b) shape

 © 2013 American Physical Society

distortions can give rise to mode splitting [21], both sources of extrinsic linewidth broadening. Therefore, measurement of the linewidth of individual nanomagnets is essential. In addition, a more systematic comparison of data with theory is made possible by examination of the dependence of damping on various spin-wave modes in nanomagnets of differing size [12–15].

Measurement of α in individual nanomagnets has been achieved with the time-resolved magneto-optical Kerr effect [22–24], but such measurements are challenging when the diffraction-limited spot size for focused visible light is much larger than the nanomagnet, adversely affecting the signal-to-noise ratio. The signal-to-noise ratio of weak optical signals can be enhanced by use of optical heterodyne detection, where the optical signal is mixed with a bright local oscillator beam [25]. We developed a novel heterodyne magneto-optical microwave microscope (H-MOMM) to measure ferromagnetic resonance (FMR) in individual, well-separated nanomagnets by use of heterodyne detection of magneto-optical signals at microwave frequencies. The signal from a spin-wave mode, e.g. the end modes in the 200 nm nanomagnets, which are localized in an $\approx 2100\ \mathrm{nm}^2$ area, measured with the H-MOMM is more than 10 times larger than measured with a conventional magneto-optical Kerr microscope. (See the Supplemental Material [26].)

Samples were prepared from thin films of $3\ \mathrm{nm\,Ta}/10\ \mathrm{nm\,Ni_{80}Fe_{20}}/5\ \mathrm{nm\,Si_3N_4}$ on 100-μm-thick sapphire substrates. Elliptical-shaped nanomagnets with nominal dimensions of $480 \times 400\ \mathrm{nm}^2$, $240 \times 200\ \mathrm{nm}^2$, and $120 \times 100\ \mathrm{nm}^2$ were patterned by e-beam and ion-mill lithography. $20 \times 20\ \mu\mathrm{m}^2$ squares were also patterned from the same films to facilitate determination of the blanket-film FMR properties (see Ref. [21] for details).

FMR spectra for two of the 400 nm nanomagnets, and three each of the 200 nm and 100 nm nanomagnets, were measured over a wide frequency range. The spectra were obtained by fixed frequency excitation and by sweeping the external magnetic field H_{ext} that was applied along the nanomagnet long axis. The microwave field from the waveguide was oriented along the short axis. The inset in Fig. 1 shows an example of a 13.2 GHz spectrum with a 100 nm magnet. As was previously demonstrated in Ref. [20], we also compared our data to micromagnetic simulations to confirm the identity of the various resonances as being associated with end- and center-mode excitations. The identification was both qualitatively and quantitatively conclusive. Further comparison of the data with micromagnetic simulations (described below) indicate that the spin-wave mode with the lowest resonance field (i.e., the ''center mode'') is distributed throughout the volume of the nanomagnet, and the two other modes (i.e. the ''end modes'') are localized at the ends of the nanomagnet along the applied field direction [20]. A perfect elliptical nanomagnet would have degenerate end modes,

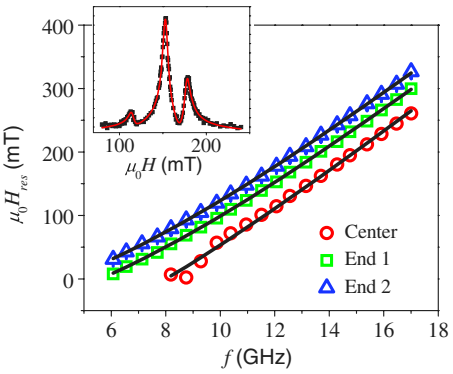

FIG. 1 (color online). Measured resonance fields for a 100 nm nanomagnet: The center mode (red circles) has the lowest resonance field followed by the end mode 1 (green squares) and end mode 2 (blue triangles). The solid lines are fits to Eq. (1). The inset shows a spectrum obtained at 13.2 GHz. The solid (red) line is a fit to Eq. (1) in the Supplemental Material [26].

but shape distortions can lift this degeneracy, as was recently demonstrated in Brillouin light scattering measurements [21]. Coupling between the end modes can also break the degeneracy, but this was determined to be negligible for the systems studied here, as discussed below.

The measured amplitudes of the end modes in the 100 nm nanomagnet are significantly larger than that of the center mode. Micromagnetic simulations (see insets in Fig. 2) indicate that the center mode actually has significant amplitude at two ends of the nanomagnet, but the precession is 180° out of phase with respect to the central part of the mode. The heterodyne signals from the center and ends have opposite signs, which leads to partial destructive interference. Additional simulations confirm that the integrated H-MOMM signals from central and end

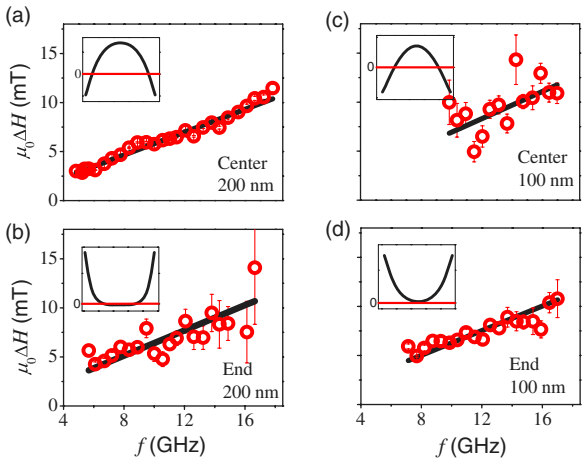

FIG. 2 (color online). Linewidths for the center modes (a) and (c) and end modes (b) and (d) for a 200 nm and a 100 nm nanomagnet. The insets show the mode profile along the long axis of the ellipsoid, as determined by micromagnetic simulations. The horizontal red line indicates zero amplitude.

portions of the center mode for the 100 nm nanomagnet should be comparable in magnitude, which explains the weak heterodyne signal from the center mode.

The measured magnitude spectra were fitted with the magnitude of the complex susceptibility χ_{xy} [27] (red line in inset of Fig. 1); see the Supplemental Material [26]. The resonance field $H_{\mathrm{res}}^{(i)}(f)$ for each mode was then fitted with the Kittel equation to extract global values for $H_1^{(i)}$ and $H_2^{(i)}$,

$$f = \left(\frac{|\gamma|\mu_0}{2\pi}\right)\sqrt{[H_{\mathrm{res}}^{(i)}(f) + H_1^{(i)}][H_{\mathrm{res}}^{(i)}(f) + H_2^{(i)}]}. \quad (1)$$

The fits of the resonance field to the frequency for the center and the two end modes for a 100 nm nanomagnet are shown in Fig. 1. The center mode has a lower resonance field and less curvature than the two end modes, while the frequency dependence of the two end modes is virtually identical except for a fixed field splitting of ≈ 25 mT for the 100 nm nanomagnets.

In the case where the two end modes are not degenerate but are coupled due to magnetostatic interactions, one might expect that modes with optical and acoustic character are excited. We used micromagnetic simulations to determine the coupling between the end modes for the 100 nm nanomagnet. Simulations yielded a mode splitting of 5 mT at 10 GHz. Appealing to a classical model of coupled, lossy harmonic oscillators [28], the effective coupling strength between two end modes is calculated to be 28 mT. Such a coupling strength is close to the experimentally observed spitting of 25 mT for the two end modes in Fig. 1. This implies that the measured modes are not purely localized at either of the two ends but instead have a degree of mixed evenlike or oddlike characters, with the excitation of one end mode necessarily driving the other end mode with a fractional amplitude of ≈ 0.08. We interpret the high field peak to be the oddlike mode and the low field peak to be the evenlike mode.

The fits of the spectra also yield the frequency dependence of the linewidth for each spin-wave mode. The linewidth of a localized spin-wave mode for a single nanomagnet does not have any contributions from inhomogeneous linewidth broadening ΔH_0 because the resonance frequency is necessarily homogenous for a single eigenmode. Moreover, extrapolation of the H-MOMM-measured linewidth data for the 20×20 μm^2 square resulted in $\mu_0 \Delta H \approx 0$ mT at $f = 0$. Thus, we can safely fit the linewidths with

$$\Delta H = (4\pi\alpha f)/(|\gamma|\mu_0). \quad (2)$$

Using Eq. (2), we extracted $\alpha = 0.0074 \pm 0.0001$ for the 20×20 μm^2 square. This value is larger than the previously reported value of 0.004 in Ref. [18]. We attribute most of the discrepancy to spin pumping at the $Ni_{80}Fe_{20}$/Ta interface [29–31]. To determine the spin-mixing conductance, we measured nearly identical, unpatterned $Ni_{80}Fe_{20}$/Ta films with thicknesses varying from 5 nm to 20 nm by broadband perpendicular FMR. This geometry eliminates two-magnon scattering for the unpatterned film [32]. The asymptotic intrinsic damping is $\alpha = 0.0050 \pm 0.0001$, in good agreement with the theoretical value $\alpha = 0.0046$ [33], and the effective spin-mixing conductance is $(1.48 \pm 0.05) \times 10^{19}$ m^{-2}. Based on these values, the predicted damping for a 10 nm film is 0.0079 ± 0.0002, in reasonable agreement with our optically measured value for the 20×20 μm^2 square. Given this agreement, we exclude two-magnon scattering as a significant source of linewidth for the optical measurements.

The measured linewidth for the nanomagnets does not exhibit a linear dependence on frequency at the lowest frequencies. This is understood because the magnetization distribution is not uniform at low applied fields. The dipolar fields near the ends of the nanomagnet are highly nonuniform, thereby inducing an inhomogeneous magnetization configuration if the applied fields are less than or equal to the dipolar fields. Such a change of the magnetization distribution also causes the resonance field for a particular excitation frequency to decrease with decreasing field. This "field-dragging" effect leads to a distortion of the resonance curve, which results in an anomalous increase in the linewidth at low frequencies. Micromagnetic simulations confirmed this behavior. To minimize the influence of the field-dragging effect on the experimentally determined α, we use a low frequency cutoff to restrict the range of linewidth data fitted to Eq. (2). (The cutoff frequency is determined by minimizing the rms error between the data and the linear fit.) Figure 2 shows the dependence of ΔH on f for the center mode and one of the end modes for a 200 nm and a 100 nm nanomagnet. The solid black lines are fits to Eq. (2).

The average values of α for the center and end modes for an ensemble of three 100 nm, three 200 nm, and two 400 nm individual nanomagnets are plotted in Fig. 3 as a function of sample size. For reference, the value of α for the 20×20 μm^2 square is shown as a thick blue line, where the estimated error in the fitted value is the width of the line. (See the Supplemental Material [26] for the α values of all measured nanomagnets.) Of particular note, α for the end mode *decreases* by almost 30% as the size of the nanomagnet is reduced from 400 nm to 100 nm, in stark contrast to what had been observed previously for the ensemble behavior of large nanomagnet arrays, where the end mode damping *increased* by 20% as the nanomagnet size in the array was reduced from 200 to 100 nm [20]. This highlights the advantage of the H-MOMM technique, whereby we can now extract the damping properties of individual structures without any obscuration due to structure-to-structure variations, which can otherwise complicate the process of extricating intrinsic damping from inhomogeneous broadening effects [21].

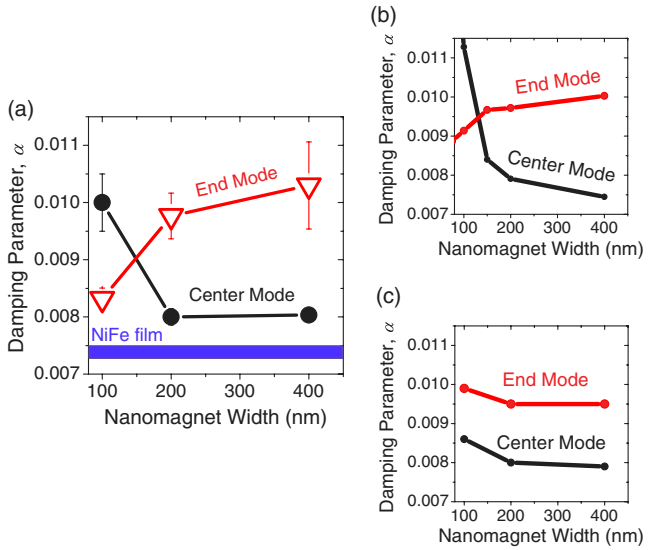

FIG. 3 (color online). (a) Experimental damping data: we plot the dependence of α on nanomagnet size. The black circles (red triangles) are the average values of the end modes (center mode). α for the 20×20 mm^2 square is marked with a blue bar, where the width of the bar indicates the measurement precision. (b) Intralayer spin-pumping model: the red circles are the fitted values of α for the end mode and the black circles for the center mode. τ_{sc} was the only fitting parameter. (c) Edge-enhanced damping model: the red circles are α for the end mode and the black circles for the center mode.

There are several different models that might explain the dependence of damping on nanomagnet size. By comparing the measured size dependence of the extracted damping to that predicted for each of the models, we show that only an increase due to nonlocal damping resulting from intralayer dissipative transverse spin currents is consistent with the experimental data. We explicitly show that damage and/or oxidation at the sidewalls of the nanomagnets cannot explain the experimental data.

Previous work [13] has predicted that longitudinal [14] and transverse [15] *intralayer* spin currents can increase the damping when the dynamics are spatially inhomogenous. The net damping torque density is given by

$$\vec{T}_{\text{damp}} = -(\alpha M_s/|\gamma|)(\vec{m} \times \partial_t \vec{m}) + (\sigma_T \vec{m} \times \nabla^2 \partial_t \vec{m}), \quad (3)$$

where $\sigma_T = (\hbar/2)^2 n_e \tau_{sc}/m^*$ is the transverse spin conductivity, n_e is the conduction electron density, m^* the effective mass, and τ_{sc} is the transverse spin scattering time, which can have contributions from momentum scattering, e-e interactions, as well as spin-orbit-induced spin-flip or decoherence processes. The Laplacian operator in Eq. (3) implies that the damping for a given Fourier component of a localized spin-wave mode is proportional to the square of the wave number. Assuming that the net damping of a given eigenmode is determined by the integral of the Laplacian for the mode, normalized by the mode area, we can use simulated mode profiles from micromagnetics to estimate the enhanced damping due to intralayer spin currents. In Fig. 3(a) we show the measured α and in 3(b) the best fit of the data, with the result $\tau_{sc} = 49$ fs as the sole fitting parameter (see the Supplemental Material [26] for details). We use $n_e = k_F^3/3\pi^2 = 3.9 \times 10^{28}$ m^{-3} from the measured Fermi wave number $k_F = 1.05 \times 10^{10}$ m^{-1} for the majority band in Permalloy [34] and the free electron mass for m^*.

The theory of nonlocal damping due to intralayer spin currents provides an intuitively appealing explanation for the decrease in damping observed for the end modes when the nanomagnet size is reduced from 200 nm to 100 nm. As the size of the nanomagnet shrinks, the two localized modes on opposite ends of the nanomagnet merge together. In doing so, as seen in the insets of Fig. 2, the combined mode becomes more uniform, thereby decreasing the components of damping that are proportional to k^2. However, micromagnetic simulations also show that the opposite is true of the center mode; shrinking the nanomagnet "squeezes" the mode structure into a smaller area, causing the mode profile to become less uniform, with the final result that the damping increases with decreasing spatial dimension.

Based on reported values for the spin diffusion length of $\ell_{sf} = 3$ nm–8 nm [35,36] and the Fermi velocity $\nu_F = 2.2 \times 10^5$ m s^{-1} [34] for Permalloy, we estimate the spin-flip time as $T_1 = \nu_F \ell_{sf} = 13$ fs–37 fs. In the degenerate limit of $T_2 = 2T_1$ where spin-flip causes spin decoherence, we estimate the maximum possible spin decoherence time as $T_2 = 26$ fs–74 fs, which bounds the fitted value we obtained for τ_{sc}.

An alternative explanation is provided by the theory of lateral diffusion of spin current generated by spin pumping into an adjacent nonmagnetic layer. However, the calculated increase in damping obtained by application of the theory in Refs. [37,38] to our micromagnetic simulation results is more than an order of magnitude smaller than what we observed.

Damage and/or oxidation at the sidewalls of a nanomagnet, which was potentially introduced during ion milling or after the patterning process, has been proposed as a source of enhanced damping [17]. To test this hypothesis, we performed micromagnetic simulations with enhanced damping at the nanomagnet edges modeled by $\alpha(y, z) = 0.0074 + \alpha' e^{-|[\sqrt{(z/\varepsilon)^2+y^2}-R]/\delta|}$, where α' is the enhanced damping at the edge, δ is the decay length, ε is the nanomagnet ellipticity, and R is the length of the short axis. We used parameter values $\alpha' = 0.003$ and $\delta = 20$ nm. The decay length was chosen to match the zone of altered contrast in transmission electron microscope images of magnetic nanostructures [39], and α' was chosen such that the simulation results match the average measured damping values for the end and center modes of the 400 nm nanomagnets. We find that the nonuniform damping profile leads to negligible mode distortions relative to

those obtained with uniform damping. The effective damping α_{eff} was determined by simulating swept-field FMR to determine ΔH, and then using Eq. (2) to extract α_{eff}, with resultant values shown in Fig. 3(c). In the case of the 400 nm and 200 nm nanomagnets, the difference in the values of damping for the end and center modes is easily accommodated with such a spatial model of edge-enhanced damping: The end mode is more localized near the edges; therefore, α_{eff} is significantly enhanced for the end modes. However, the model breaks down in the case of the 100 nm nanomagnets. While simulations predict that α_{eff} increases, the data clearly show that the damping for the 100 nm nanomagnet end mode is significantly less than the end mode damping for both the 200 nm and the 400 nm nanomagnets. Thus, edge damage fails to explain the observed trend for α.

Therefore, we conclude that our measured values for α for discrete spin-wave eigenmodes in individual, isolated nanomagnets are well explained by the theory of nonlocal damping due to intralayer dissipative transverse spin currents.

We would like to thank Y. Tserkovnyak, M. Schneider, and M. Donahue for helpful discussions.

[1] L. Landau and E. Lifshitz, Phys. Z. Sowjetunion **8**, 153 (1935).
[2] T. L. Gilbert and J. M. Kelly, *Conference on Magnetism and Magnetic Materials, Pittsburgh, 1955* (American Institute of Electrical Engineers, New York, 1955), p. 253–263.
[3] T. L. Gilbert, IEEE Trans. Magn. **40**, 3443 (2004).
[4] J.-G. Zhu, X. Zhu, and Y. Tang, IEEE Trans. Magn. **44**, 125 (2008).
[5] S. Kaka, M. R. Pufall, W. H. Rippard, T. J. Silva, S. E. Russek, and J. A. Katine, Nature (London) **437**, 389 (2005).
[6] E. Mirowski, J. Moreland, A. Zhang, S. E. Russek, and M. J. Donahue, Appl. Phys. Lett. **86**, 243901 (2005).
[7] "International Technology Roadmap for Semiconductors 2011, Emerging Research Devices," http://www.itrs.net/Links/2011ITRS/Home2011.htm.
[8] V. Kamberský, Czechoslovak Journal of Physics, Section B **26**, 1366 (1976).
[9] K. Gilmore, Y. U. Idzerda, and M. D. Stiles, Phys. Rev. Lett. **99**, 027204 (2007).
[10] K. Gilmore and M. D. Stiles, Phys. Rev. B **79**, 132407 (2009).
[11] R. Urban, G. Woltersdorf, and B. Heinrich, Phys. Rev. Lett. **87**, 217204 (2001).
[12] J. Foros, A. Brataas, Y. Tserkovnyak, and G. E. W. Bauer, Phys. Rev. B **78**, 140402(R) (2008).
[13] C. H. Wong and Y. Tserkovnyak, Phys. Rev. B **80**, 184411 (2009).
[14] S. Zhang and S. S.-L. Zhang, Phys. Rev. Lett. **102**, 086601 (2009).
[15] Y. Tserkovnyak, E. M. Hankiewicz, and G. Vignale, Phys. Rev. B **79**, 094415 (2009).
[16] G. D. Fuchs, J. C. Sankey, V. S. Pribiag, L. Qian, P. M. Braganca, A. G. F. Garcia, E. M. Ryan, Z.-P. Li, O. Ozatay, D. C. Ralph, and R. A. Buhrman, Appl. Phys. Lett. **91**, 062507 (2007).
[17] O. Ozatay, P. G. Gowtham, K. W. Tan, J. C. Read, K. A. Mkhoyan, M. G. Thomas, G. D. Fuchs, P. M. Braganca, E. M. Ryan, K. V. Thadani, J. Silcox, D. C. Ralph, and R. A. Buhrman, Nat. Mater. **7**, 567 (2008).
[18] H. M. Olson, P. Krivosik, K. Srinivasan, and C. E. Patton, J. Appl. Phys. **102**, 023904 (2007).
[19] M. L. Schneider, J. M. Shaw, A. B. Kos, T. Gerrits, T. J. Silva, and R. D. McMichael, J. Appl. Phys. **102**, 103909 (2007).
[20] J. M. Shaw, T. J. Silva, M. L. Schneider, and R. D. McMichael, Phys. Rev. B **79**, 184404 (2009).
[21] H. T. Nembach, J. M. Shaw, T. J. Silva, W. L. Johnson, S. A. Kim, R. D. McMichael, and P. Kabos, Phys. Rev. B **83**, 094427 (2011).
[22] B. Rana, D. Kumar, S. Barman, S. Pal, Y. Fukuma, Y. Otani, and A. Barman, ACS Nano **5**, 9559 (2011).
[23] P. S. Keatley, P. Gangmei, M. Dvornik, R. J. Hicken, J. R. Childress, and J. A. Katine, Appl. Phys. Lett. **98**, 082506 (2011).
[24] I. Neudecker, F. Hoffmann, G. Woltersdorf, and C. H. Back, J. Phys. D **41**, 164010 (2008).
[25] A. T. Forrester, J. Opt. Soc. Am. **51**, 253 (1961).
[26] See Supplemental Material at http://link.aps.org/supplemental/10.1103/PhysRevLett.110.117201 for a detailed description of the heterodyne magneto-optical microscope and the fitting procedure for the H-MOMM spectra, calculation of the contribution of the intralayer spincurrents to the damping, and a table providing the damping parameter α for all the measured spin-wave modes.
[27] H. T. Nembach, T. J. Silva, J. M. Shaw, M. L. Schneider, M. J. Carey, S. Maat, and J. R. Childress, Phys. Rev. B **84**, 054424 (2011).
[28] K. R. Symon, *Mechanics* (Addision-Wesley, New York, 1971).
[29] Y. Tserkovnyak, A. Brataas, and G. E. W. Bauer, Phys. Rev. Lett. **88**, 117601 (2002).
[30] T. Gerrits, M. L. Schneider, and T. J. Silva, J. Appl. Phys. **99**, 023901 (2006).
[31] B. Heinrich, Y. Tserkovnyak, G. Woltersdorf, A. Brataas, R. Urban, and G. E. W. Bauer, Phys. Rev. Lett. **90**, 187601 (2003).
[32] R. Arias and D. L. Mills, Phys. Rev. B **60**, 7395 (1999).
[33] A. A. Starikov, P. J. Kelly, A. Brataas, Y. Tserkovnyak, and G. E. W. Bauer, Phys. Rev. Lett. **105**, 236601 (2010).
[34] D. Y. Petrovykh, K. N. Altmann, H. Hochst, M. Laubscher, S. Maat, G. J. Mankey, and F. J. Himpsel, Appl. Phys. Lett. **73**, 3459 (1998).
[35] T. Kimura, J. Hamrle, and Y. Otani, Phys. Rev. B **72**, 014461 (2005).
[36] F. J. Jedema, M. S. Nijboer, A. T. Filip, and B. J. van Wees, Phys. Rev. B **67**, 085319 (2003).
[37] Y. Tserkovnyak, A. Brataas, G. E. W. Bauer, and B. I. Halperin, Rev. Mod. Phys. **77**, 1375 (2005).
[38] M. L. Polianski and P. W. Brouwer, Phys. Rev. Lett. **92**, 026602 (2004).
[39] J. W. Lau, X. Liu, R. C. Boling, and J. M. Shaw, Phys. Rev. B **84**, 214427 (2011).